



Effect of Gd content on microstructure and dynamic mechanical properties of solution-treated Mg–xGd–3Y–0.5Zr alloy

Xue-zhao WANG¹, You-qiang WANG^{1,2}, Chen-bing NI¹, Yu-xin FANG¹, Xiao YU¹, Ping ZHANG³

1. School of Mechanical and Automotive Engineering, Qingdao University of Technology, Qingdao 266520, China;
2. Key Lab of Industrial Fluid Energy Conservation and Pollution Control, Ministry of Education, Qingdao 266520, China;
3. College of Mechanical and Electronic Engineering, Shandong University of Science and Technology, Qingdao 266590, China

Received 22 July 2021; accepted 26 October 2021

Abstract: The effect of Gd content ranging from 6.5 wt.% to 8.5 wt.% on microstructure evolution and dynamic mechanical behavior of Mg–xGd–3Y–0.5Zr alloys was investigated by optical microscopy, X-ray diffraction, scanning electron microscopy and split Hopkinson pressure bar. The microstructure of as-cast Mg–xGd–3Y–0.5Zr alloys indicates that the addition of Gd can promote grain refinement in the casting. Due to the rapid cooling rate during solidification, a large amount of non-equilibrium eutectic phase Mg₂₄(Gd,Y)₅ appears at the grain boundary of as-cast Mg–xGd–3Y–0.5Zr alloys. After solution treatment at 520 °C for 6 h, the Mg₂₄(Gd,Y)₅ phase dissolves into the matrix, and the rare earth hydrides (REH) phase appears. The stress–strain curves validate that the solution-treated Mg–xGd–3Y–0.5Zr alloys with optimal Gd contents maintain excellent dynamic properties at different strain rates. It was concluded that the variation of Gd content and the agglomeration of residual REH particles and dynamically precipitated fine particles are key factors affecting dynamic mechanical properties of Mg–xGd–3Y–0.5Zr alloys.

Key words: Mg–xGd–3Y–0.5Zr alloy; microstructure; dynamic mechanical properties; rare earth hydrides; dynamic precipitated phase

1 Introduction

Magnesium with abundant resource reserves is the lightest engineering metal material in the manufacturing industry, which is known as the green engineering material of the 21st century [1,2]. Due to its outstanding physical and mechanical performance, such as low density, high specific strength, high specific stiffness and good damping performance, magnesium and its alloys have been successfully and widely used in the fields of the aerospace, transportation and electronic products [3–6]. However, the critical issue of low

absolute mechanical strength makes it challenging to meet the increasingly stringent requirements of modern industries, which has become a dominant obstacle restricting the widespread application of the magnesium and its alloys.

The improvement of the microstructure and mechanical properties of magnesium-based alloys has attracted the close attention of many scholars. Previous studies [7–11] have demonstrated that the suitable addition of Gd, Y and Nd elements to magnesium alloys can significantly improve the mechanical strength of the alloys, thereby preparing high-strength magnesium-based rare earth alloys. Recently, with the excellent mechanical properties,

Corresponding author: You-qiang WANG, Tel: +86-18660279607, E-mail: wq1970301@126.com;
Chen-bing NI, Tel: +86-17866829775, E-mail: nichenbing@126.com

DOI: 10.1016/S1003-6326(22)65939-9

1003-6326/© 2022 The Nonferrous Metals Society of China. Published by Elsevier Ltd & Science Press

the Mg–Gd–Y system rare-earth alloy has become a new generation of light alloy material research hotspot. SU et al [7] found that the extruded-T5 Mg–2.5Gd–0.75Y–0.5Zn–0.3Mn alloy exhibited superior ultimate tensile strength of 520 MPa at room temperature. HOMMA et al [8] concluded that the ultimate tensile strength, the yield strength and the elongation to failure of the high-strength Mg–1.8Gd–1.8Y–0.7Zn–0.2Zr alloy fabricated by extrusion and aging process are 542 MPa, 473 MPa and 8.0%, respectively. MA et al [9] reported that the tensile strength of the high-strength Mg–8.5Gd–4Y–1Zn–0.4Zr alloy prepared by centrifugal casting and ring rolling process reaches 511 MPa. Therefore, the Mg–Gd–Y-based alloys with high mechanical strength can be widely employed to fabricate lightweight structural parts.

Currently, the concept of lightweight design is highly acknowledged in energy conservation and equipment performance improvement. For lightweight design, high-strength aluminum alloy materials such as 2519A, 7039 and 2139 are widely used in the production of armored vehicles and commercial vehicles. The ultimate tensile strength of high-strength aluminum alloys usually ranges from 480 to 550 MPa [12–14]. Comparing the mechanical properties between aforementioned magnesium alloys and high-strength aluminum alloys, it is clear that the Mg–Gd–Y-based alloys with light weight and high strength can be anticipated to be one of the important alternative materials for structural parts in lightweight design. The dynamic compressive properties of Mg–Gd–Y-based alloys are generally investigated through the split Hopkinson pressure bar experiment. YU et al [15] and MAO et al [16] found that the extruded Mg–Gd–Y alloys have excellent impact resistance at room and high temperatures, and their dynamic compressive strength exceeds 510 MPa. Besides, the mechanical properties of the Mg–Gd–Y alloys with different aging precipitation phases were investigated in our group. It was concluded that the aging precipitation phase is of great significance to improve the mechanical properties of the alloys [17,18].

The chemical composition and elemental ratio are of great significance to the microstructure and mechanical properties of the alloys. Thus, the research work done by scholars in the research of Mg–Gd–Y-based alloy can be mainly classified

into two aspects: one is the addition of other alloying elements for this family [19–22]; the other is the optimization of main alloying element content in this department [23–25]. Therefore, the abundant research work is concentrated on the composition design and optimization of Mg-based alloy, which has established a solid foundation for the fabrication of high-performance Mg-based alloy. In addition, the existing research mainly focuses on the effect of chemical composition on the static mechanical performance of Mg-based alloy. However, the effects of chemical composition on the dynamic mechanical behavior, as well as the mechanism of microstructure evolution on dynamic mechanical properties are still unclear. With the widespread application of Mg-based alloy in engineering, the increasingly stringent requirements are put forward for its dynamic mechanical properties. Consequently, in this work, the effect of Gd content ranging from 6.5 wt.% to 8.5 wt.% on the microstructure evolution and dynamic mechanical properties of Mg–xGd–3Y–Zr alloy are investigated, and the influence of second-phase particles including the residual rare earth-rich particles after the solution treatment and dynamically precipitated fine particles during SPHB tests on the dynamic mechanical properties are analyzed and discussed.

2 Experimental

The preparation of Mg–Gd–Y-based alloy ingots in this study was carried out in a resistance furnace, where magnesium was added in the form of pure magnesium and alloying elements Gd, Y and Zr were added in the form of Mg–Gd, Mg–Y and Mg–Zr intermediate alloys, respectively. Then, the Mg–Gd–Y–Zr alloys were melted, refined and poured. A protective argon atmosphere was employed to prevent oxidation throughout the melting process. The main chemical composition of the designed Mg–xGd–3Y–0.5Zr alloys is designed as listed in Table 1.

The samples for optical microscopy (OM) and scanning electron microscopy (SEM) observation were prepared by sandpaper grinding and mirror polishing according to the standard metallographic preparation methods, and then etched in a solution of 4.0% (volume fraction) HNO₃ solution with ethanol. SEM observation was performed on a

ZEISS EVO MA10 with an acceleration voltage of 10 kV. The chemical composition of the second-phase was analyzed by the equipped energy dispersive spectrometer (EDS). X-ray diffraction (XRD) was conducted on a Bruker D8A A25 diffractometer with Cu K_{α} radiation.

Table 1 Chemical composition of designed Mg–xGd–3Y–0.5Zr alloys (wt.%)

Alloy No.	Gd	Y	Zr	Mg
I	6.5	3	0.5	Bal.
II	7.5	3	0.5	Bal.
III	8.5	3	0.5	Bal.

The dynamic compression test of Mg–xGd–3Y–0.5Zr alloys was carried out on a split Hopkinson pressure bar (SHPB) system at room temperature. The samples with a height of 4.0 mm and a diameter of 6.0 mm were cut from the plate using a wire electric discharge machine. To ensure the mechanical strength and ductility of the Mg–xGd–3Y–0.5Zr alloys, the ingots were first treated by solution treatment at 520 °C for 6 h and then cooled in the water. In addition, the impact surfaces of the specimens were polished with metallographic sandpaper before SHPB tests. The sample was placed between the incident bar and the transmission bar, and the loading direction was parallel to the extrusion direction in the sample clamp.

3 Results

3.1 Microstructure evolution

The metallographic microstructure of the as-cast Mg–xGd–3Y–0.5Zr alloys with different Gd contents is shown in Fig. 1. It can be found that the grain size shows a decreasing trend with the increase of Gd content during the casting and forming process of Mg–xGd–3Y–0.5Zr alloys. The average grain sizes of Mg–xGd–3Y–0.5Zr alloys with Gd mass fractions of 6.5 wt.%, 7.5 wt.%, and 8.5 wt.% are about 38.0, 32.5 and 30.9 μm , respectively, which are calculated by the truncated line method. Thus, the rare earth element Gd has the effect of promoting grain refinement in the casting process of Mg–xGd–3Y–0.5Zr alloys. Besides, some black particles with approximate spherical geometry can be observed in the

microstructure of Mg–xGd–3Y–0.5Zr alloys, as shown in Fig. 1. According to the research of literature [26,27], the approximately spherical structure particles are Zr-rich particles. Zr and Mg possess the identical hexagonal close packed crystal structure and almost same lattice constants (discrepancy <1.3%). In addition, Zr has a relatively low solid solubility in Mg-based alloy, which is not conducive to the formation of any intermetallic phase. Thus, Zr-rich particles can also promote grain refinement in casting process of Mg-based alloys [28].

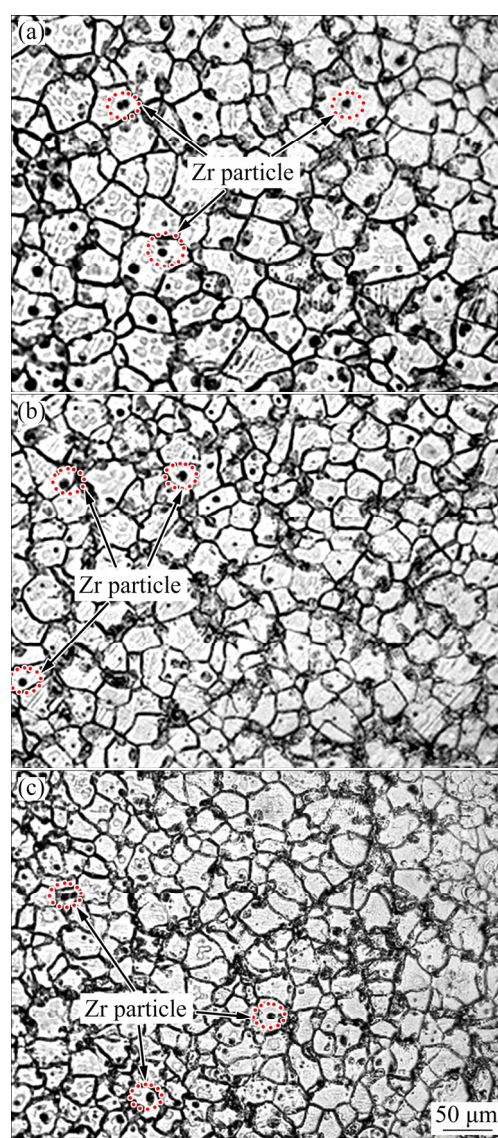


Fig. 1 Optical microscopy images of as-cast Mg–xGd–3Y–0.5Zr alloys: (a) $x=6.5$; (b) $x=7.5$; (c) $x=8.5$

High-magnification SEM images and semi-quantitative EDS analysis were conducted to further determine the grain distribution features and the

composition of the second-phase in as-cast Mg– x Gd–3Y–0.5Zr alloys, as given in Fig. 2. The black second-phase and Zr-rich particles in metallographic photographs in Fig. 1 are bright white under the SEM. It can be observed that some second-phase particles with skeletal shape appear at the grain boundary of as-cast Mg– x Gd–3Y–0.5Zr alloys. With the increase of Gd content, the amount of the skeletal second-phase in as-cast Mg– x Gd–3Y–0.5Zr alloys presents a growth trend, while the size of the second-phase exhibits a decreasing trend. Based on the EDS results in Figs. 2(d) and (f), the skeletal second-phase (Zones A and C) is rich in rare earth elements Gd and Y, where the mass fractions of Gd and Y elements are about 35 wt.% and 7 wt.%, respectively.

The phase analysis of the as-cast Mg– x Gd–3Y–0.5Zr alloys was performed by XRD to determine the existing state of the second-phase, as shown in Fig. 3. Through the comparison of the PDF card, the diffraction pattern of the as-cast Mg– x Gd–3Y–0.5Zr alloys is composed of the magnesium matrix phase and the Mg₂₄Gd₅ phase (PDF No. 31-0817). Because the nature of the Gd element is similar to that of the Y element, some Y atoms usually replace Gd atoms in the Mg₂₄Gd₅ phase. Therefore, according to previous EDS analysis results of the second-phase in Fig. 2 and the XRD pattern results in Fig. 3, it can be

determined that the existing state of the second-phase at the grain boundary can be expressed as Mg₂₄(Gd,Y)₅. The skeletal-like Mg₂₄(Gd,Y)₅ is a body-centered cubic (BCC) structure with a lattice constant of $a=1.126$ nm, which is consistent with the findings of literature [29,30]. The non-equilibrium eutectic phase Mg₂₄(Gd,Y)₅ is generated by high cooling rates during the solidification of Mg– x Gd–3Y–0.5Zr alloys, which can be eliminated by solid solution treatment later.

The metallographic structure and EDS results of the Mg– x Gd–3Y–0.5Zr alloys after solution treatment at 520 °C for 6 h are illustrated in Fig. 4. The results indicate that after the solution treatment, the non-equilibrium eutectic phase Mg₂₄(Gd,Y)₅ generated at the grain boundary of as-cast Mg– x Gd–3Y–0.5Zr alloys fully dissolves into the matrix, and only a small amount of white square-shaped second-phase particles and Zr-rich particles remain at the grain boundary. It can be found in Figs. 4(a)–(c) that the number of white square-shaped second-phase particles tends to increase gradually with the increase of Gd content. In particular, when the mass fraction of Gd is 8.5 wt.%, the white square-shaped second-phase particles in the metallographic structure exhibit agglomeration, while the size of square-shaped second-phase particles tends to decrease. According to the EDS results of white square-shaped particles

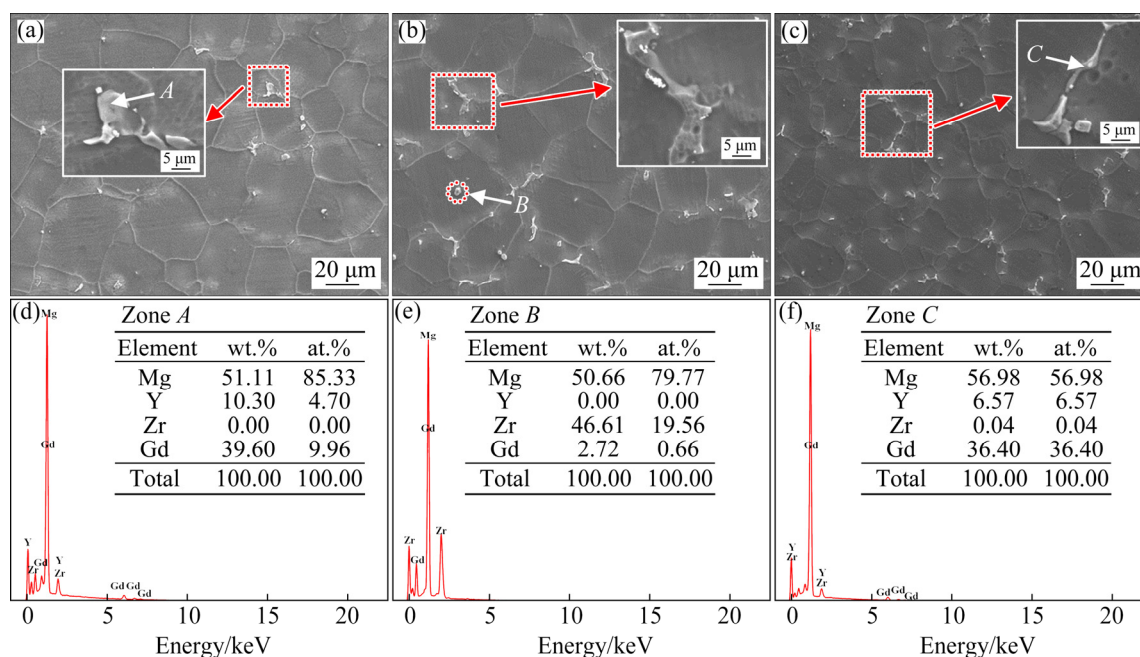


Fig. 2 SEM images (a, b, c) and EDS results (d, e, f) of as-cast Mg– x Gd–3Y–0.5Zr alloys: (a) $x=6.5$; (b) $x=7.5$; (c) $x=8.5$; (d) Zone A; (e) Zone B; (f) Zone C

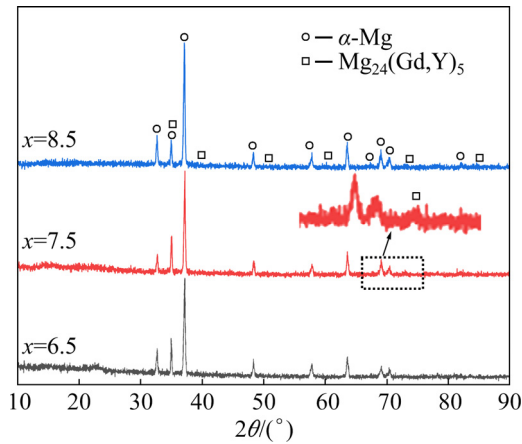


Fig. 3 XRD patterns of as-cast Mg- x Gd-3Y-0.5Zr alloys with different Gd contents

in Figs. 4(d)–(f), it can be obtained that there are significant differences in the Gd and Y element contents of the square-shaped second-phase particles in the solution-treated Mg- x Gd-3Y-0.5Zr alloys. The research [31] demonstrated that the white square-shaped second-phase particles are rare earth hydrides (REH) formed during the solid solution of Mg-RE-based alloys. The REH particles have a face-centered cubic (FCC) structure with a lattice constant of $a=0.56$ nm.

Furthermore, the XRD patterns of the solution-treated Mg- x Gd-3Y-0.5Zr alloys was performed to determine the dissolution of the non-equilibrium

eutectic phase Mg₂₄(Gd,Y)₅, as shown in Fig. 5. It can be seen that the diffraction peaks of the non-equilibrium eutectic phase Mg₂₄(Gd,Y)₅ disappear after the solution-treated Mg- x Gd-3Y-0.5Zr alloys. Therefore, according to the SEM images and the EDS analysis results in Fig. 4, it can be concluded that the non-equilibrium eutectic phase Mg₂₄(Gd,Y)₅ at the grain boundary has been fully dissolved into the matrix after solution treatment.

3.2 Dynamic mechanical performance

The macro morphologies of the solution-treated Mg- x Gd-3Y-0.5Zr alloys after SHPB tests are illustrated in Fig. 6. It can be observed that when the strain rate reaches 3705 s⁻¹, obvious impact cracks occur on the solution-treated Mg-6.5Gd-3Y-0.5Zr alloy specimen. Subsequently, more serious impact cracks appear in the solution-treated Mg-6.5Gd-3Y-0.5Zr alloy sample when the strain rate reaches 4033 s⁻¹. Compared with the macro morphology of Mg-6.5Gd-3Y-0.5Zr alloy at the high strain rates of 3705 and 4033 s⁻¹, only slight impact cracks appear at the edge of the Mg- x Gd-3Y-0.5Zr samples with Gd contents of 7.5 wt.% and 8.5 wt.% at the high strain rates of 3895 and 3995 s⁻¹. Therefore, compared with dynamic mechanical properties of Mg-6.5Gd-3Y-0.5Zr alloy, the compression resistance of Mg- x Gd-3Y-0.5Zr alloys with Gd content of 7.5 wt.%

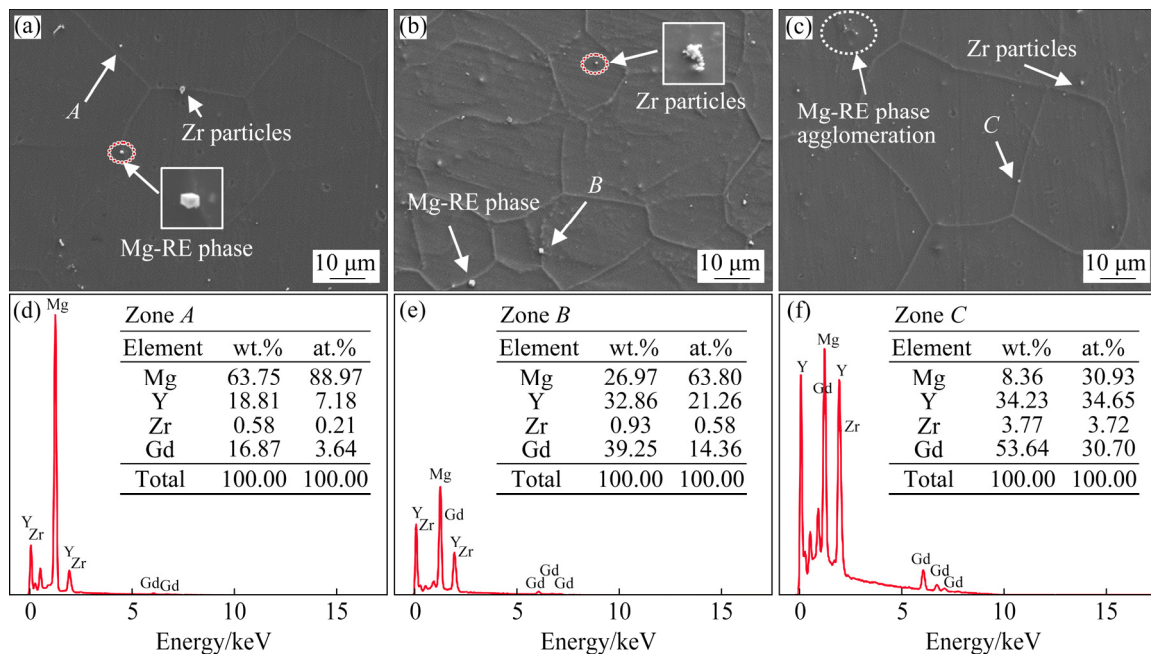


Fig. 4 SEM images (a, b, c) and EDS results (d, e, f) of solution-treated Mg- x Gd-3Y-0.5Zr alloys with different Gd contents: (a) $x=6.5$; (b) $x=7.5$; (c) $x=8.5$; (d) Zone A; (e) Zone B; (f) Zone C

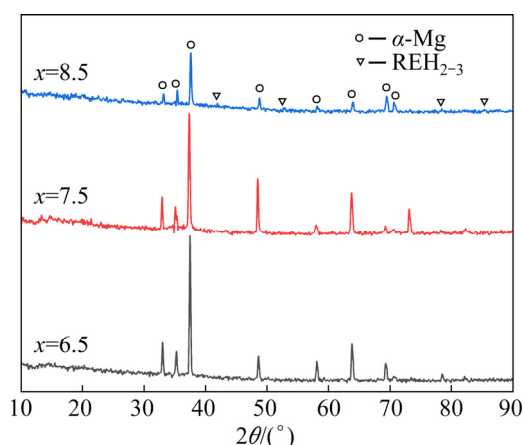


Fig. 5 XRD patterns of solution-treated Mg- x Gd-3Y-0.5Zr alloys with different Gd contents

and 8.5 wt.% is significantly improved. Besides, the angle between the impact crack and the compression direction is approximately 45° , as shown in Fig. 6(a). According to the principles of mechanics, the main tangent plane of the cylindrical specimen is 45° with the compression direction

under the action of dynamic impact pressure, therefore, the fracture occurs along the main tangent plane of the sample during the dynamic impact. Moreover, when the strain rate is extremely high in SHPB tests, the cracks initiate and propagate rapidly in different main tangent planes resulting in the cone-shaped fracture morphology, as shown in Fig. 6(a) at the strain rate of 4033 s^{-1} .

The stress-strain curves of the solution-treated Mg- x Gd-3Y-0.5Zr alloys derived from SHPB tests at room temperature are shown in Fig. 7. The effects of Gd content on the ultimate compressive strength and yield strength of the solution-treated Mg- x Gd-3Y-0.5Zr alloys at different strain rates are shown in Fig. 8. It can be obtained that the solution-treated Mg- x Gd-3Y-0.5Zr alloys with different Gd contents exhibit excellent impact resistance in SHPB tests. The compressive strength and yield strength of the solution-treated Mg-6.5Gd-3Y-0.5Zr alloy first increase and then decrease with the increase of strain rate. And the maximum compressive strength of the solution-



Fig. 6 Photographs of solution-treated Mg- x Gd-3Y-0.5Zr samples after dynamic compression under different strain rates: (a) $x=6.5$; (b) $x=7.5$; (c) $x=8.5$

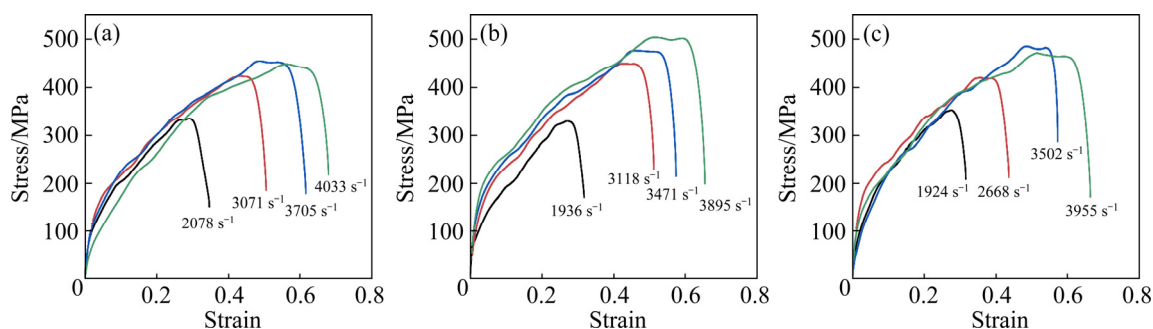


Fig. 7 Dynamic compressive stress-strain curves of solution-treated Mg- x Gd-3Y-0.5Zr samples: (a) $x=6.5$; (b) $x=7.5$; (c) $x=8.5$

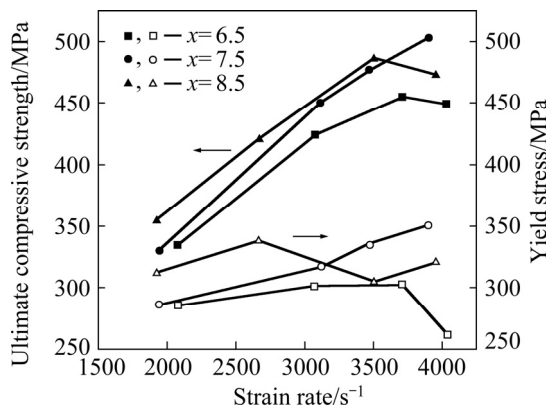


Fig. 8 Dynamic mechanical properties of solution-treated Mg- x Gd-3Y-0.5Zr samples with different Gd contents

treated Mg-6.5Gd-3Y-0.5Zr alloy reaches 455 MPa at the strain rate of 3705 s⁻¹. According to macro-fracture morphology, the premature fracture of the solution-treated Mg-6.5Gd-3Y-0.5Zr sample is the fundamental reason for the decrease of compressive strength at high strain rates.

Under the designed strain parameters, the compressive strength and yield strength of the solution-treated Mg-7.5Gd-3Y-0.5Zr alloy exhibit a monotonically growing trend with the increase of strain rate. The maximum compressive strength of 503 MPa and yield strength of 351 MPa occur in the solution-treated Mg-7.5Gd-3Y-0.5Zr alloy at the strain rate of 3895 s⁻¹. Compared with the performance of solution-treated Mg-6.5Gd-3Y-0.5Zr alloy, the impact resistance and yield strength of solution-treated Mg-7.5Gd-3Y-0.5Zr sample is significantly improved. The improvement of compressive strength and yield strength can be attributed to the refinement of grain and the uniformity of microstructure with the increase of Gd content.

The variation of dynamic mechanical properties of the solution-treated Mg-8.5Gd-3Y-0.5Zr alloy is similar to that of the alloy with 6.5 wt.% Gd. The overall compressive strength of the solution-treated Mg-8.5Gd-3Y-0.5Zr alloy at different strain rates is significantly improved except for the compressive strength at the strain rate of 3955 s⁻¹. This can be attributed to the agglomeration phenomenon of the square-shape second-phase in the microstructure resulting in premature fracture. The maximum compressive strength of the solution-treated Mg-8.5Gd-3Y-0.5Zr alloy reaches 486 MPa at the strain rate of

3502 s⁻¹. The yield strength of Mg-8.5Gd-3Y-0.5Zr alloy increases significantly at low strain rates. However, the yield strength of Mg-8.5Gd-3Y-0.5Zr alloy decreases significantly when the strain rate is greater than 2668 s⁻¹, which is related to the effect of the square-shape second-phase on its plasticity [32]. In short, the variation of Gd content and the agglomeration of the second-phase particles are the main factors affecting the dynamic mechanical properties of Mg- x Gd-3Y-0.5Zr alloys.

Furthermore, the stress-strain curves of the solution-treated Mg- x Gd-3Y-0.5Zr samples exhibit a slight jitter characteristic indicating the serrated yield phenomenon of the material in SHPB. The jitter phenomenon is more pronounced when the Gd content is 8.5 wt.%. The jitter phenomenon of the stress-strain curves is consistent with the Portevin-Le Chatelier cluster effect [33], which is caused by the dynamic strain aging property of the material. The solute atoms become an obstacle to the dislocation of the solvent atom during the rapid deformation of the material. When the velocity of solute atom is lower than that of dislocation movement, i.e., pegging dislocation, the solute atom will hinder the dislocation movement. However, when the dislocation movement speed is extremely high, the phenomenon of debonding occurs. Therefore, the slight jitter phenomenon occurs in the stress-strain curves of the solution-treated Mg- x Gd-3Y-0.5Zr alloy samples in SHPB tests.

4 Discussion

4.1 Micro-morphology analysis

The micro-morphology of Mg- x Gd-3Y-0.5Zr alloys is shown in Fig. 9 after the dynamic compression with relatively low strain rates ranging from 1924 to 2078 s⁻¹. Both the volume fraction and size of the precipitated second-phase particles decrease significantly with the increase of Gd content. The agglomeration of square-shaped second-phase particles occurs in the Mg-6.5Gd-3Y-0.5Zr alloys. Figure 9(d) shows that the content of Gd is the highest reaching 45 wt.%, and the Y content is 39 wt.%, both of which are greater than the Mg matrix with 10 wt.%. Comparing to the microstructure and EDS results of Mg-6.5Gd-3Y-0.5Zr samples before dynamic compression shown

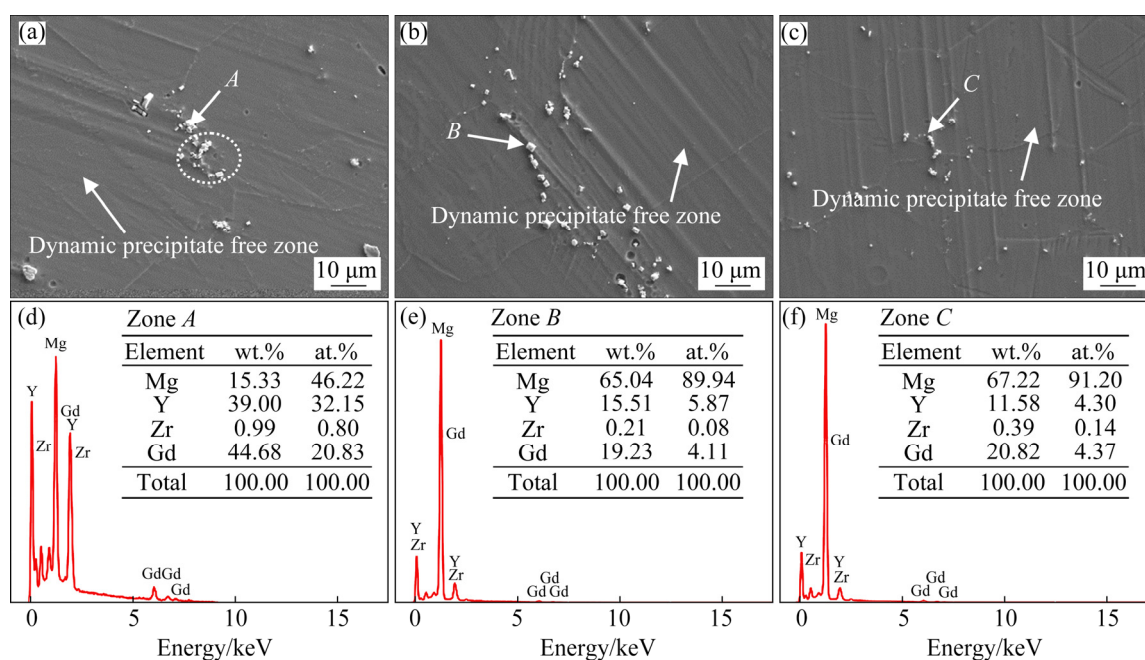


Fig. 9 Micro-morphologies (a, b, c) and EDS results (d, e, f) of Mg-xGd-3Y-0.5Zr alloys after SHPB tests under low strain rates: (a) $x=6.5$, 2078 s^{-1} ; (b) $x=7.5$, 1936 s^{-1} ; (c) $x=8.5$, 1924 s^{-1} ; (d) Zone A; (e) Zone B; (f) Zone C

in Fig. 4, it is clear that the square-shaped second-phase is the residual rare earth-rich particles after the solution treatment. Besides, some fine second-phase particles are distributed around the coarse massive particles, as shown by arrows B and C in Fig. 9. The EDS results indicate that the fine second-phase particles are composed of 20 wt.% Gd and 15 wt.% Y. According to the research of literature [34], the energy spectrum results of fine second-phase particles are consistent with those of the dynamic precipitation particles. Moreover, it can be observed in Figs. 9(a-c) that the number of the square-shaped second-phase particles decreases while the number of fine second-phase particles increases with the increase of Gd content. This indicates that Mg-xGd-3Y-0.5Zr alloys undergo dynamic precipitation during the dynamic impact process. The dynamically precipitated particles and the square-shaped second-phase particles hinder the movement of dislocations to a certain extent, which allows the alloy to maintain high impact resistance.

Figure 10 presents the micro-morphology of Mg-xGd-3Y-0.5Zr alloys after the dynamic compression with medium strain rates ranging from 3471 to 3705 s^{-1} . Similar to the case given in Fig. 9, the square-shaped RE-rich particles and fine second-phase particles can be observed. Thus, it can be concluded that the stable RE-rich particles do

not dissolve into the matrix during high-strain dynamic impact. According to the micro-morphology and EDS results of fine second-phase particles, the dynamic precipitation phenomenon occurs in the moderate speed dynamic impact process of Mg-xGd-3Y-0.5Zr alloys. Nevertheless, the number of dynamically precipitated particles at moderate strain rates ranging from 3471 to 3705 s^{-1} increases significantly with respect to that at low strain rates ranging from 1924 to 2078 s^{-1} . The fine dynamic precipitated particles are mainly concentrated near the square-shaped RE-rich phase, and there are no dynamic precipitated particles in the region far away from RE-rich particles. This can be attributed to the hindering effect of the RE-rich particles on dislocations, resulting in a large number of dislocations to accumulate around them. Therefore, the dynamic precipitation only occurs in near RE-rich particles in the microstructure of Mg-xGd-3Y-0.5Zr alloys. In addition, the streak-like second-phase appears in the microstructure of Mg-xGd-3Y-0.5Zr alloys with 8.5 wt.% Gd shown in Fig. 10(c). According to the EDS analysis results in Fig. 10(f), the observed streak-like second-phase is the aggregation phenomenon of Zr-rich particles, which is beneficial to hindering the dislocation movement and improve the impact resistance of Mg-8.5Gd-3Y-0.5Zr alloys.

Figure 11 shows the micro-morphology of Mg- x Gd-3Y-0.5Zr alloys after the dynamic compression with high strain rates ranging from 3895 to 4033 s⁻¹. Compared with the amount of dynamically precipitated particles in Fig. 10, it can be found that the dynamic precipitation amount of Mg- x Gd-3Y-0.5Zr alloys is relatively reduced overall, which can be attributed to the extremely short deformation time under high-strain dynamic

impact. As shown in Fig. 11(a), a great number of microcracks occur in the microstructure of Mg-6.5Gd-3Y-0.5Zr alloys at a strain rate of 4033 s⁻¹. The EDS results in Fig. 11(d) indicate that the second-phase precipitated in the middle of microcracks has a very high Gd content of 85.1 wt.%. The second-phase with extremely high Gd content results in the premature fracture and deterioration of the mechanical properties of

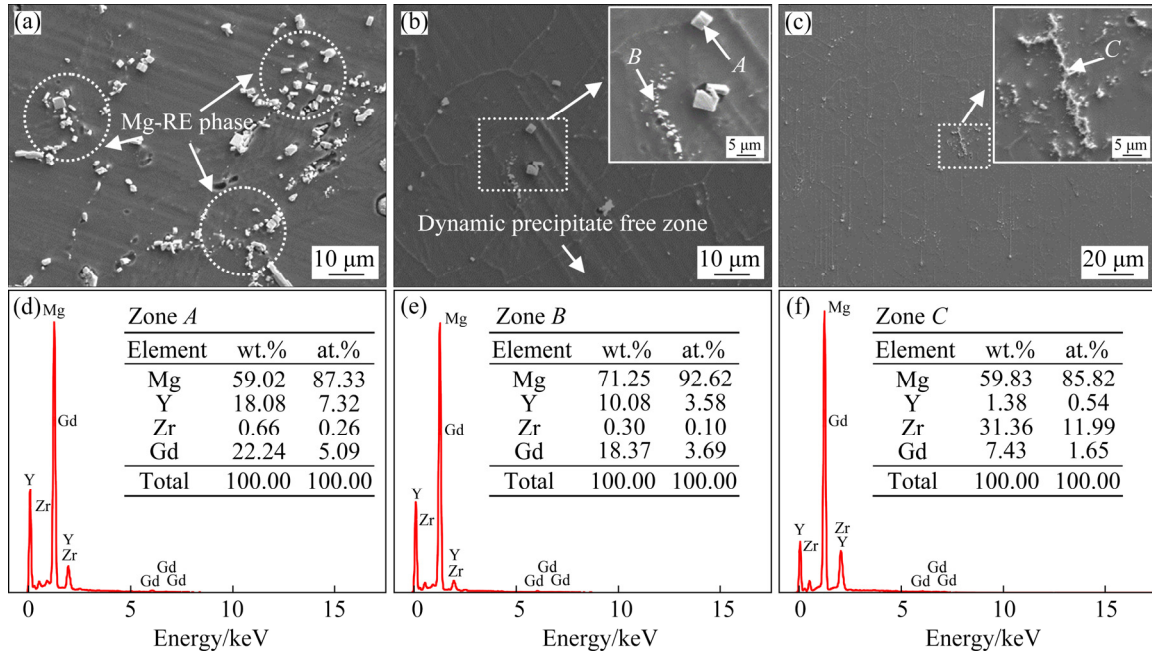


Fig. 10 Micro-morphologies (a, b, c) and EDS results (d, e, f) of Mg- x Gd-3Y-0.5Zr alloys after SHPB tests under medium strain rates: (a) $x=6.5$, 3705 s⁻¹; (b) $x=7.5$, 3471 s⁻¹; (c) $x=8.5$, 3502 s⁻¹; (d) Zone A; (e) Zone B; (f) Zone C

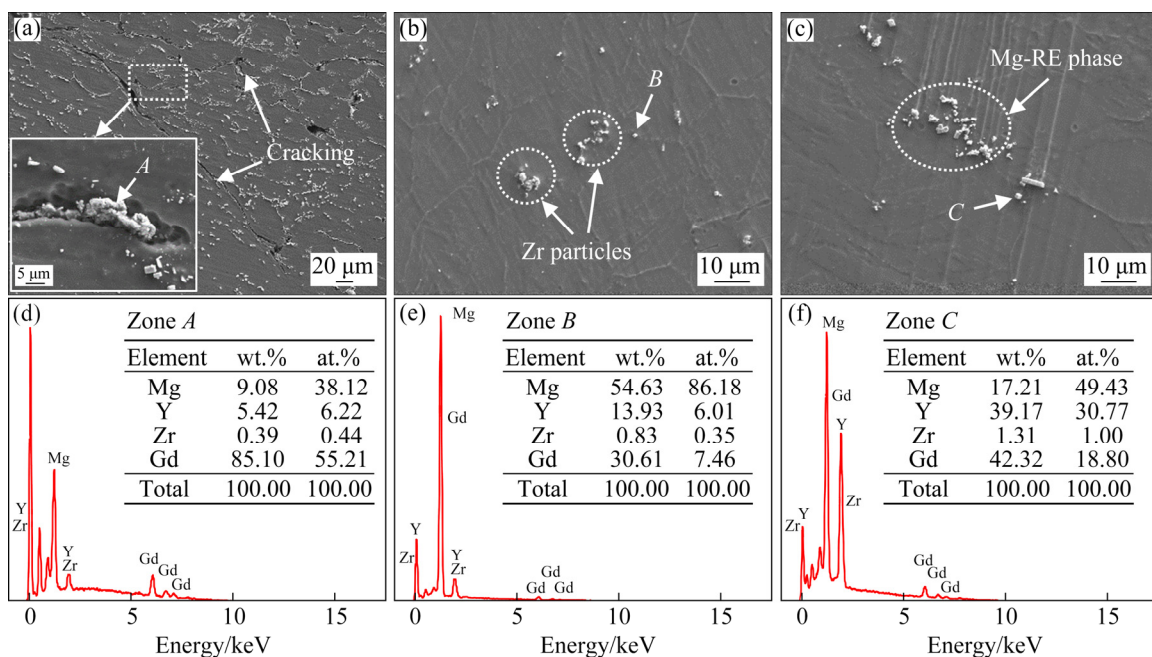


Fig. 11 Micro-morphologies (a, b, c) and EDS results (d, e, f) of Mg- x Gd-3Y-0.5Zr alloys after SHPB tests under high strain rates: (a) $x=6.5$, 4033 s⁻¹; (b) $x=7.5$, 3895 s⁻¹; (c) $x=8.5$, 3955 s⁻¹; (d) Zone A; (e) Zone B; (f) Zone C

Mg–6.5Gd–3Y–0.5Zr alloys. The amount of dynamic precipitation particles is obviously reduced in Mg–7.5Gd–3Y–0.5Zr alloy as shown in Fig. 11(b). However, the agglomeration of Zr-rich particles occurs in Mg–7.5Gd–3Y–0.5Zr alloys at a strain rate of 3895 s^{-1} , which allows the alloy to maintain excellent impact resistance. There are few fine particles precipitated dynamically in Mg–8.5Gd–3Y–0.5Zr alloy at a strain rate of 3955 s^{-1} except for some larger square particles, as shown in Fig. 11(c). The agglomeration of large block particles leads to stress concentration, which has a negative effect on the mechanical properties of Mg–8.5Gd–3Y–0.5Zr alloys.

4.2 Adiabatic temperature rise analysis

During the dynamic impact process, most of the kinetic energy of the incident bar is dissipated in the form of thermal energy, and only a few percent of the energy is stored in the material in the form of phase interface energy, dislocation energy and elastic strain energy [35]. In a very short time, a large amount of heat generated in the high-speed impact process is difficult to dissipate before the deformation process is completed. As a result, the local temperature of the samples will rise rapidly.

The absorbed energy (W) per unit volume of material can effectively evaluate the adiabatic temperature rise of the sample during the dynamic compression process. The absorption energy (W) can be calculated by [36]

$$W = \int \sigma d\varepsilon \quad (1)$$

where σ and ε denote the stress and strain of the material during dynamic compression, respectively.

According to the dynamic compression stress–strain curves, the absorption energy values of the Mg– x Gd–3Y–0.5Zr alloys under different deformation conditions were calculated, as given in Table 2. The adiabatic temperature rise (ΔT) during the dynamic compression process can be quantitatively calculated according to Eq. (2) [35]:

$$\Delta T = \frac{\beta}{\rho c_v} \int \sigma d\varepsilon \quad (2)$$

where β represents the conversion factor between work and heat, and $\beta=1$; c_v represents the specific heat capacity and $c_v=1000 \text{ J/(kg}\cdot\text{°C)}$; ρ represents the density and $\rho=1.90\times 10^3 \text{ kg/m}^3$. The calculated results of the adiabatic temperature rise of the Mg– x Gd–3Y–0.5Zr alloys under different

deformation conditions are shown in Table 3. Obviously, the adiabatic temperature rise of the Mg– x Gd–3Y–0.5Zr alloys compressed at high strain rates is significantly higher than that of the samples compressed at low strain rates.

Table 2 Calculation results of absorption energy (W) of Mg– x Gd–3Y–0.5Zr alloys

Deformation condition	$W/(\text{MJ}\cdot\text{m}^{-3})$
$x=6.5, 2078 \text{ s}^{-1}$	82.52
$x=6.5, 4033 \text{ s}^{-1}$	219
$x=7.5, 1936 \text{ s}^{-1}$	72.44
$x=7.5, 3895 \text{ s}^{-1}$	251.59
$x=8.5, 1924 \text{ s}^{-1}$	80.08
$x=8.5, 3955 \text{ s}^{-1}$	237.12

Table 3 Calculation results of adiabatic temperature rise (ΔT) of Mg– x Gd–3Y–0.5Zr alloys

Deformation condition	$\Delta T/^\circ\text{C}$
$x=6.5, 2078 \text{ s}^{-1}$	43.43
$x=6.5, 4033 \text{ s}^{-1}$	115.26
$x=7.5, 1936 \text{ s}^{-1}$	38.13
$x=7.5, 3895 \text{ s}^{-1}$	132.42
$x=8.5, 1924 \text{ s}^{-1}$	42.15
$x=8.5, 3955 \text{ s}^{-1}$	124.8

It can be found in Table 3 that the adiabatic temperature rise of Mg–7.5Gd–3Y–0.5Zr alloy is lower than that of magnesium alloys with Gd content of 6.5 wt.% and 8.5 wt.% at low strain rates. The stress–strain curves and dynamic mechanical properties in Figs. 7 and 8 show that the mechanical properties of Mg–7.5Gd–3Y–0.5Zr alloy are slightly inferior to those of the other two alloys. This can be attributed to the fact that relatively long deformation time and low adiabatic temperature rise at low strain rates cannot effectively suppress the generation of dynamic precipitation. The micro-morphology of Mg– x Gd–3Y–0.5Zr alloys after SHPB tests at low strain rates in Fig. 9 also verified the results that the dynamic precipitates of Mg–7.5Gd–3Y–0.5Zr alloy are obviously more than those of other alloys. As shown in Table 3, the adiabatic temperature rise of Mg– x Gd–3Y–0.5Zr alloys at high strain rates is significantly higher than that of the alloys at low strain rates. Contrary to the low strain rate, the adiabatic temperature

rise of Mg–7.5Gd–3Y–0.5Zr alloy reaches the maximum of 132.42 °C at high strain rates. The high adiabatic temperature rise that can effectively inhibit the dynamic precipitation is the key reason for the excellent dynamic mechanical properties of the Mg–xGd–3Y–0.5Zr alloy at high strain rates. In addition, the effective deformation time of samples at high strain rates is significantly less than that at low strain rates. Therefore, the high adiabatic temperature rise and the short deformation period are important factors for the suppressed dynamic precipitation behavior under high strain rates.

5 Conclusions

(1) The grain size shows a decreasing trend with the increase of Gd content during the casting and forming process of Mg–xGd–3Y–0.5Zr alloys. The average grain sizes of Mg–xGd–3Y–0.5Zr alloys with Gd mass fractions of 6.5 wt.%, 7.5 wt.%, and 8.5 wt.% are about 38.0, 32.5 and 30.9 μm, respectively.

(2) The non-equilibrium eutectic Mg₂₄(Gd,Y)₅ appears at the grain boundary of as-cast Mg–xGd–3Y–0.5Zr alloys because of the high cooling rate during solidification. The square-shaped rare earth hydrides (REH) appear at the grain boundary, while the second-phase Mg₂₄(Gd,Y)₅ with skeletal shape dissolves into the matrix after the solution treatment at 520 °C for 6 h.

(3) The ultimate compressive strength and yield strength of Mg–xGd–3Y–0.5Zr alloys present an increasing trend with the increase of Gd content and strain rate in SHPB tests. The Mg–xGd–3Y–0.5Zr alloy with 7.5 wt.% Gd exhibits better comprehensive dynamic mechanical properties than the alloys with 6.5 wt.% and 8.5 wt.% Gd. The maximum compressive strength of 503 MPa and yield strength of 351 MPa occur in the solution-treated Mg–7.5Gd–3Y–0.5Zr alloy at the strain rate of 3895 s⁻¹.

(4) The variation of Gd content and the agglomeration of the second-phase particles are main factors affecting the dynamic mechanical properties of Mg–xGd–3Y–0.5Zr alloys. The residual square-shaped particles after solution treatment and the precipitated fine particles in SHPB hinder the movement of dislocations to a certain extent, which allows the alloys to maintain excellent impact resistance.

Acknowledgments

This study was supported by the National Natural Science Foundation of China (Nos. 51575289, 51705270), the Key Research and Development Project of Shandong Province, China (No. 2019GHY112068), and the Natural Science Foundation of Shandong Province, China (No. ZR2019PEE028).

References

- [1] PAN Fu-sheng, YANG Ming-bo, CHEN Xian-hua. A review on casting magnesium alloys: Modification of commercial alloys and development of new alloys [J]. *Journal of Materials Science & Technology*, 2016, 32: 1211–1221.
- [2] XU Shi-yuan, LIU Chu-ming, WAN Ying-chun, ZENG Guang, GAO Yong-hao, JIANG Shu-nong. Corrosion behaviour of Mg–Gd–Y–Zn–Ag alloy components with different sizes after cooling [J]. *Transactions of Nonferrous Metals Society of China*, 2021, 31: 1291–1302.
- [3] ZHANG Xin-ming, TANG Chang-ping, DENG Yun-lai, YANG Liu, LIU Wen-jun. Phase transformation in Mg–8Gd–4Y–Nd–Zr alloy [J]. *Journal of Alloys and Compounds*, 2011, 509: 6170–6174.
- [4] LI Li, ZHANG Xin-ming. Microstructure and texture evolution during high-strain-rate superplastic deformation of coarse-grained Mg–Gd–Y–Zr rolled sheet [J]. *Transactions of Nonferrous Metals Society of China*, 2011, 21: 1491–1497.
- [5] YOU Chao, LIU Chu-ming, WAN Ying-chun, TANG Bei, WANG Bi-zheng, GAO Yong-hao, HAN Xiu-zhu. Dislocations-induced precipitates and their effect on mechanical properties of Mg–Gd–Y–Zr alloy [J]. *Journal of Magnesium and Alloys*, 2019, 7: 414–418.
- [6] JIA Qing-gong, ZHANG Wen-xin, SUN Yi, XU Chun-xiang, ZHANG Jin-shan, KUAN Jun. Microstructure and mechanical properties of as-cast and extruded biomedical Mg–Zn–Y–Zr–Ca alloy at different temperatures [J]. *Transactions of Nonferrous Metals Society of China*, 2019, 29: 515–525.
- [7] SU Ning, WU Yu-juan, DENG Qing-chen, CHANG Zhi-yu, WU Qian-ye, XUE Yan-ting, YANG Kun, CHEN Qiang, PENG Li-ming. Synergic effects of Gd and Y contents on the age-hardening response and elevated-temperature mechanical properties of extruded Mg–Gd(–Y)–Zn–Mn alloys [J]. *Materials Science and Engineering A*, 2021, 810: 141019.
- [8] HOMMA T, KUNITO N, KAMADO S. Fabrication of extraordinary high-strength magnesium alloy by hot extrusion [J]. *Scripta Materialia*, 2009, 61: 644–647.
- [9] MA Zhen-duo, LI Guo, PENG Qiang, PENG Xiao-dong, CHEN Dao-lun, ZHANG Han-zhu, YANG Yan, WEI Guo-bing, XIE Wei-dong. Microstructural evolution and enhanced mechanical properties of Mg–Gd–Y–Zn–Zr alloy via centrifugal casting, ring-rolling and aging [J]. *Journal of Magnesium and Alloys*, 2022, 10: 119–128.

- [10] TANG Chang-ping, WANG Xue-zhao, LIU Wen-hui, FENG Di, WU Kai, ZHANG Chao, MIAO Guo-dong, LIANG Wu-ying, LI Jing, LIU Xiao, LI Quan. Effects of thermomechanical processing on the microstructure, texture and mechanical properties of a Mg–Gd-based alloy [J]. *Materials Science and Engineering A*, 2019, 759: 172–180.
- [11] OUYANG Si-jie, LIU Wen-cai, WU Guo-hua, JI Hao, GAO Zhan-kui, PENG Xiang, LI Zhong-quan, DING Wen-jiang. Microstructure and mechanical properties of as-cast Mg–8Li–xZn–yGd (x=1, 2, 3, 4; y=1, 2) alloys [J]. *Transactions of Nonferrous Metals Society of China*, 2019, 29: 1211–1222.
- [12] LIU Wen-hui, HE Zhen-tao, CHEN Yu-qiang, TANG Si-wen. Dynamic mechanical properties and constitutive equations of 2519A aluminum alloy [J]. *Transactions of Nonferrous Metals Society of China*, 2014, 24: 2179–2186.
- [13] SUN Da-xiang, ZHANG Xin-ming, YE Ling-ying, GUI Xing-hui, JIANG Hai-chun, GU Gang. Comparative study of the dynamic mechanical behavior of aluminum alloy 2519A and 7039 [J]. *Materials Science and Engineering A*, 2015, 640: 165–170.
- [14] KIM S, JO M C, PARK T W, HAM J, SOHN S S, LEE S. Correlation of dynamic compressive properties, adiabatic shear banding, and ballistic performance of high-strength 2139 and 7056 aluminum alloys [J]. *Materials Science and Engineering A*, 2021, 804: 140757.
- [15] YU Jin-cheng, LIU Zheng, DONG Yang, WANG Zhi. Dynamic compressive property and failure behavior of extruded Mg–Gd–Y alloy under high temperatures and high strain rates [J]. *Journal of Magnesium and Alloys*, 2015, 3: 134–141.
- [16] MAO Ping-li, YU Jin-cheng, LIU Zheng, DONG Yang. Microstructure evolution of extruded Mg–Gd–Y magnesium alloy under dynamic compression [J]. *Journal of Magnesium and Alloys*, 2013, 1: 64–75.
- [17] TANG Chang-ping, WANG Xue-zhao, LIU Wen-hui, FENG Di, ZUO Guo-liang, LI Dong, LI Xiao-yuan, CHEN Xu, LI Quan, LIU Xiao. Effect of deformation conditions on dynamic mechanical behavior of a Mg–Gd-based alloy [J]. *Journal of Materials Engineering and Performance*, 2020, 29: 8414–8421.
- [18] TANG Chang-ping, WU Kai, LIU Wen-hui, FENG Di, ZUO Guo-liang, LIANG Wu-ying, YANG Yue, CHEN Xu, LI Quan, LIU Xiao. Dynamic compression behavior of a Mg–Gd-based alloy at elevated temperature [J]. *Metals and Materials International*, 2021, 27: 1438–1447.
- [19] GUAN Li-qun, DENG Yun-lai, LUO An, GUO Xiao-bin, TANG Chang-ping. Activation of $\langle c+a \rangle$ slip and enhanced ductility in as-extruded Mg–Gd–Y–Nd alloys through Si addition [J]. *Materials Science and Engineering A*, 2021, 804: 140736.
- [20] DING Zhi-bing, ZHAO Yu-hong, LU Ruo-peng, YUAN Mei-ni, WANG Zhi-jun, LI Hui-jun, HOU Hua. Effect of Zn addition on microstructure and mechanical properties of cast Mg–Gd–Y–Zr alloys [J]. *Transactions of Nonferrous Metals Society of China*, 2019, 29: 722–734.
- [21] NAJAFI S, MAHMUDI R. Enhanced microstructural stability and mechanical properties of the Ag-containing Mg–Gd–Y alloys [J]. *Journal of Magnesium and Alloys*, 2020, 8: 1109–1119.
- [22] JIA Lin-yue, DU Wen-bo, WANG Zhao-hui, LIU Ke, LI Shu-bo, YU Zi-jian. Dual phases strengthening behavior of Mg–10Gd–1Er–1Zn–0.6Zr alloy [J]. *Transactions of Nonferrous Metals Society of China*, 2020, 30: 635–646.
- [23] JAFARI NODOOSHAN H R, WU Guo-hua, LIU Wen-cai, WEI Guang-ling, LI Yan-lei, ZHANG Song. Effect of Gd content on high temperature mechanical properties of Mg–Gd–Y–Zr alloy [J]. *Materials Science and Engineering A*, 2016, 651: 840–847.
- [24] JAFARI NODOOSHAN H R, LIU Wen-cai, WU Guo-hua, RAO You, ZHOU Chen-xu, HE Shi-peng, DING Wen-jiang, MAHMUDI R. Effect of Gd content on microstructure and mechanical properties of Mg–Gd–Y–Zr alloys under peak-aged condition [J]. *Materials Science and Engineering A*, 2014, 615: 79–86.
- [25] TANG Chang-ping, WU Kai, LIU Wen-hui, FENG Di, WANG Xue-zhao, MIAO Guo-dong, YANG Mao-mao, LIU Xiao, LI Quan. Effects of Gd, Y content on the microstructure and mechanical properties of Mg–Gd–Y–Nd–Zr alloy [J]. *Metals*, 2018, 8: 790.
- [26] WANG Cheng-qi, SUN Ming, ZHENG Fei-yan, PENG Li-ming, DING Wen-jiang. Improvement in grain refinement efficiency of Mg–Zr master alloy for magnesium alloy by friction stir processing [J]. *Journal of Magnesium and Alloys*, 2014, 2: 239–244.
- [27] TONG Xin, WU Guo-hua, ZHANG Liang, LIU Wen-cai, DING Wen-jiang. Achieving low-temperature Zr alloying for microstructural refinement of sand-cast Mg–Gd–Y alloy by employing zirconium tetrachloride [J]. *Materials Characterization*, 2021, 171: 110727.
- [28] QIAN Ma, STJOHN D H. Grain nucleation and formation in Mg–Zr alloys [J]. *International Journal of Cast Metals Research*, 2009, 22: 256–259.
- [29] LI Ji-lin, CHEN Rong-shi, KE Wei. Microstructure and mechanical properties of Mg–Gd–Y–Zr alloy cast by metal mould and lost foam casting [J]. *Transactions of Nonferrous Metals Society of China*, 2011, 21: 761–766.
- [30] GUO Yong-chun, LI Jian-ping, LI Jin-shan, YANG Zhong, ZHAO Juan, XIA Feng, LIANG Min-xian. Mg–Gd–Y system phase diagram calculation and experimental clarification [J]. *Journal of Alloys and Compounds*, 2008, 450: 446–451.
- [31] ZHU Su-ming, NIE Jian-feng, GIBSON M A, EASTON M A. On the unexpected formation of rare earth hydrides in magnesium–rare earth casting alloys [J]. *Scripta Materialia*, 2014, 77: 21–24.
- [32] HUANG Yuan-ding, YANG Lei, YOU Si-hang, GAN Wei-min, KAINER K U, HORT N. Unexpected formation of hydrides in heavy rare earth containing magnesium alloys [J]. *Journal of Magnesium and Alloys*, 2016, 4: 173–180.
- [33] KOVÁCS Z S, CHINH N Q, LENDVAI J, VÖRÖS G. Portevin-Le Châtelier type plastic instabilities in depth sensing macro-indentation [J]. *Materials Science and Engineering A*, 2002, 325: 255–260.
- [34] TANG Chang-ping, LIU Wen-hui, CHEN Yu-qiang, LIU Xiao, DENG Yun-lai. Effects of thermal treatment on microstructure and mechanical properties of a Mg–Gd-based alloy plate [J]. *Materials Science and Engineering A*, 2016,

659: 63–75.

[35] KAPOOR R, NEMAT-NASSER S. Determination of temperature rise during high strain rate deformation [J]. Mechanics of Materials, 1998, 27: 1–12.

[36] HU Shen-yang, BASKES M I, STAN M, CHEN Long-qing. Atomistic calculations of interfacial energies, nucleus shape and size of θ' precipitates in Al–Cu alloys [J]. Acta Materialia, 2006, 54: 4699–4707.

Gd 含量对固溶处理 Mg–xGd–3Y–0.5Zr 合金组织与动态力学性能的影响

王雪兆¹, 王优强^{1,2}, 倪陈兵¹, 房玉鑫¹, 于晓¹, 张平³

1. 青岛理工大学 机械与汽车工程学院, 青岛 266520;

2. 工业流体节能与污染控制教育部重点实验室, 青岛 266520;

3. 山东科技大学 机械电子工程学院, 青岛 266590

摘要: 采用金相显微镜、X 射线衍射、扫描电子显微镜、分离式霍普金森压杆等手段, 研究 Gd 含量(6.5%~8.5%, 质量分数)对 Mg–xGd–3Y–0.5Zr 合金显微组织与动力学行为的影响。观察铸态 Mg–xGd–3Y–0.5Zr 合金显微组织可知, Gd 的加入可促进晶粒细化。由于合金凝固时冷却速度快, 在晶界处出现大量非平衡共晶相 Mg₂₄(Gd,Y)₅。经过 520 °C 固溶处理 6 h 后, 非平衡共晶相 Mg₂₄(Gd,Y)₅ 融入基体中并产生稀土氢化物相(REH)。根据应力–应变曲线可知, 不同 Gd 含量的固溶态 Mg–xGd–3Y–0.5Zr 合金在不同应变速率下均表现出优异的抗冲击性能。结果表明, Gd 含量的变化、稀土氢化物粒子的聚集以及细小的动态析出相是影响 Mg–xGd–3Y–0.5 Zr 合金动态力学性能的关键因素。

关键词: Mg–xGd–3Y–0.5Zr 合金; 显微组织; 动态力学性能; 稀土氢化物; 动态析出相

(Edited by Xiang-qun LI)